## Supporting Information

# Supercapattery-driven electrolyzer both empowered by the same superb electrocatalyst

*Thangavel Kavinkumar, Selvaraj Seenivasan, Amarnath T. Sivagurunathan and Do-Heyoung Kim**

School of Chemical Engineering, Chonnam National University, 77 Yongbong-ro, Gwangju 61186, Republic of Korea.

*Corresponding author's email: kdhh@chonnam.ac.kr

Tel. (office): +82-62-530-1894

## Experimental section

***Synthesis of $CuCo_2O_4$ nanoneedles:*** Typically, $CoCl_2 \cdot 6H_2O$ (2 mM), $CuCl_2 \cdot 6H_2O$ (1 mM), and urea (20 mM) were dissolved in 40 mL of deionized (DI) water under stirring. Cleaned NF was immersed in the as-prepared reaction mixture. The above solution was then transferred into a 100 mL Teflon autoclave and maintained at 120 °C for 10 h. Finally, the resulting $CuCo_2O_4$-coated NF was annealed at 300 °C under a $N_2$ atmosphere. The obtained $CuCo_2O_4$ was rinsed with DI water and ethanol and then dried at 70 °C for further use.

***Synthesis of the Encapsulated $CuCo_2O_4$/MoNi:*** Typically, 1 mmol $Ni(NO_3)_2 \cdot 6H_2O$, 1 mmol $Na_2MoO_4 \cdot 2H_2O$, and 7.5 mmol urea were mixed in 40 mL of DI water under stirring. Then, a piece of NF coated with the $CuCo_2O_4$ was then immersed in the reaction mixture. Then, it was

transferred to a 100 mL Teflon-lined autoclave and kept at 150°C for 3 h. Then, the product was washed with DI water and ethanol and dried at 60°C. The $CuCo_2O_4$/MoNi were obtained by annealing the above prepared sample in a $H_2$/Ar (5:95) atmosphere at 500 °C for 2 h.

***Preparation of NiO encapsulated $CuCo_2O_4$/MoNi:*** Thin NiO layers were deposited over the $CuCo_2O_4$/MoNi architecture on NF via 420 deposition cycles using a laboratory-built flow-type ALD reactor.[1] During deposition, the temperature was maintained at 175 °C.

***Characterizations***

XRD data of the samples were recorded by a Rigaku X-ray diffractometer X-ray diffractometer with CuKα radiation. The morphologies and microstructures of the samples were investigated by FE-SEM (JEOL JSM-7500F) and TEM (TECNAI G2 F20 TEM system). XPS was performed on an ESCALAB-MKII, VG Scientific Co. system. The Brunauer-Emmett-Teller (BET, ASAP2010, Micromeritics) was done to measure surface area of the prepared products.

**Water splitting measurements**

Electrocatalytic properties of the as-prepared samples on the NF were carried out in a three-electrode cell, where SCE and Pt foil were employed as the reference and counter, electrodes using the electrochemical workstation (WonATech WBCS30000), respectively. Additionally, 5 mg of Pt/C (or $RuO_2$) and 10 μL of Nafion were dispersed in 1 mL of a water/alcohol mixture solution (3:1) using ultrasonication to prepare an ink. Finally, 50 μL of the catalyst ink was coated on NF and dried at 60°C. Additionally, LSV measurements were performed at 2 mV $s^{-1}$ for the OER and HER in a 1 M KOH. The EIS measurement were conducted using a Parstat 3000 workstation (0.01 Hz to 100 kHz with a 10 mV amplitude). A gas

chromatography (074-594-P1E Micro GC Fusion, INFICON) was used to analyze the amount of the gaseous products. All potentials were calibrated to the RHE using Eq. 1; η was obtained using Eq. 2 and the Tafel slope was obtained using Eq. 3:

$$E_{RHE} = E_{SCE} + 0.059pH + 0.247, \quad (1)$$

$$\eta = E_{RHE} - 1.23, \quad (2)$$

$$\eta = b \log j + a . \quad (3)$$

**Supercapattery measurements**

The electrochemical capacitive properties of the as-prepared heterostructure electrodes were carried out in 2 M KOH aqueous solution using a three-electrode cell. The as-fabricated materials on NF, Pt foil and SCE were employed as the working, counter and reference electrodes, respectively. The mass loading of the NiO@$CuCo_2O_4$/MoNi/$MoO_2$ heterostructure and AC were measured to be 4.3 and 5.4 mg $cm^{-2}$, respectively. In the supercapattery cell, the NiO@$CuCo_2O_4$/MoNi/$MoO_2$ heterostructure electrode used as the cathode and AC as the anode with 2M KOH/PVA gel as the electrolyte.

Specific capacitance ($C_s$, F $g^{-1}$) and specific capacity ($C_m$, C $g^{-1}$) from GCD test was calculated by using the relation,[2, 3]

$$C_s = \frac{2i/V\, dt}{m\,(V_f - V_i)^2} \quad (4)$$

$$C_m = C_s \times \Delta V \quad (5)$$

where, m (g), i (A), ($V_f$-$V_i$), and $\int V\,dt$ are the mass of the active materials coated on NF, applied current, functional potential frame, and the integral area of discharge curve, respectively.

The energy density (E) and power density (P) of the supercapattery were calculated according to the following formulas:

$$E = \frac{I \int V\,dt}{3.6} \qquad (6)$$

$$P = \frac{3600 \times E}{t} \qquad (7)$$

Where I (A $g^{-1}$) and t (s) are the current density, and discharge time of the supercapattery cell, respectively.

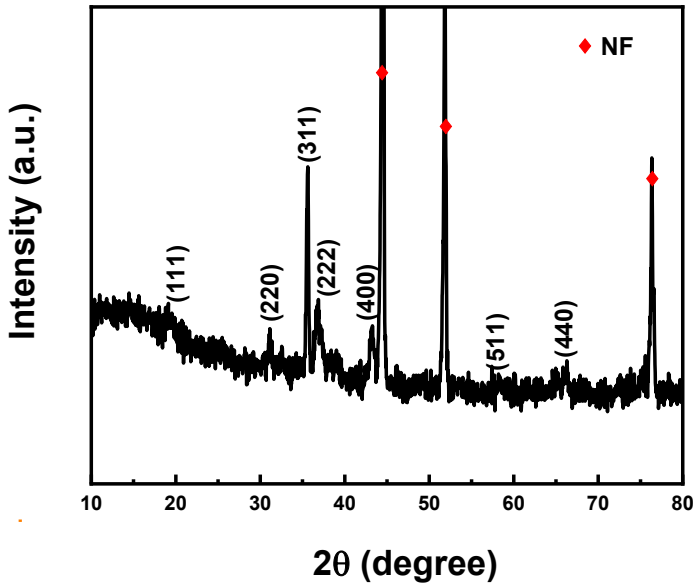


**Figure S1.** XRD pattern of the $CuCo_2O_4$ nano-needle from the NF substrate.

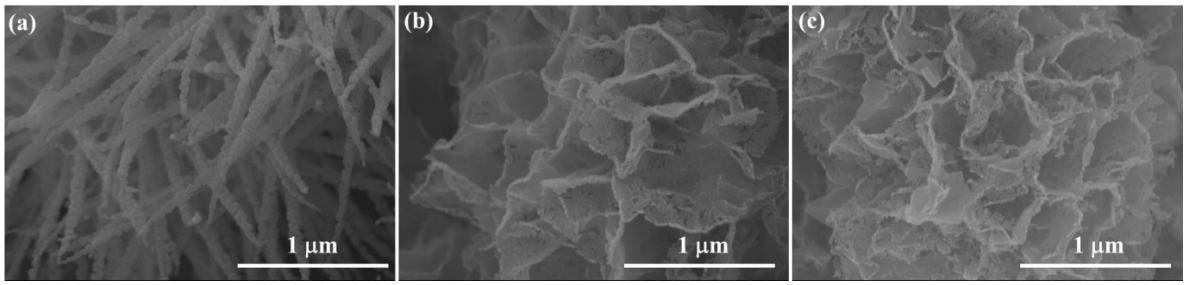


**Figure S2.** FE-SEM images of a) $CuCo_2O_4$, b) MoNi, and c) $CuCo_2O_4$/MoNi.

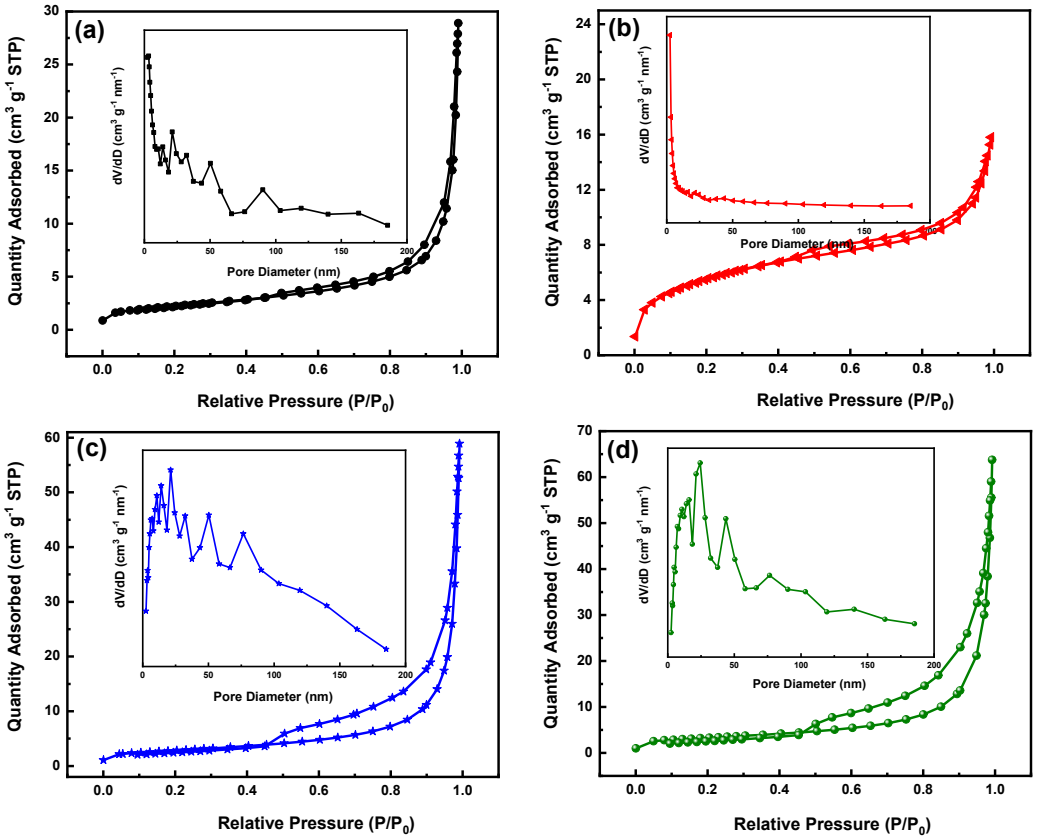


**Figure S3.** $N_2$ adsorption-desorption isotherms of a) $CuCo_2O_4$, b) MoNi, c) $CuCo_2O_4$/MoNi and d) NiO@$CuCo_2O_4$/MoNi heteronanostructure. Inset shows corresponding pore size distribution profiles.

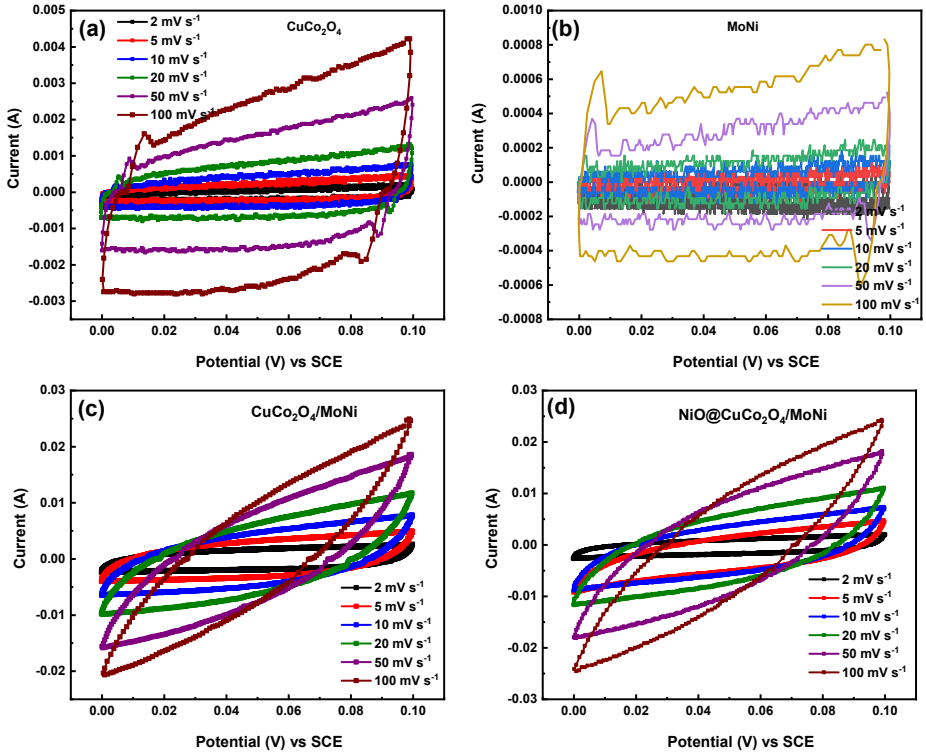


**Figure S4.** CV profiles of a) $CuCo_2O_4$, b) MoNi, c) $CuCo_2O_4$/MoNi and d) NiO@$CuCo_2O_4$/MoNi at different sweep rates in 1 M KOH.

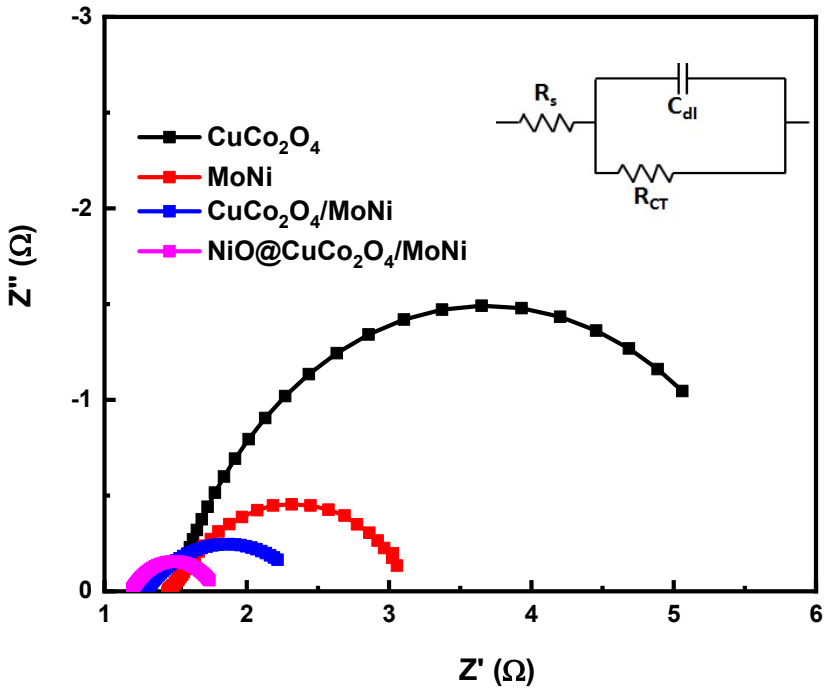


**Figure S5.** Nyquist plots for the as-prepared samples at -0.2 V. The inset shows the electrochemical equivalent circuit.

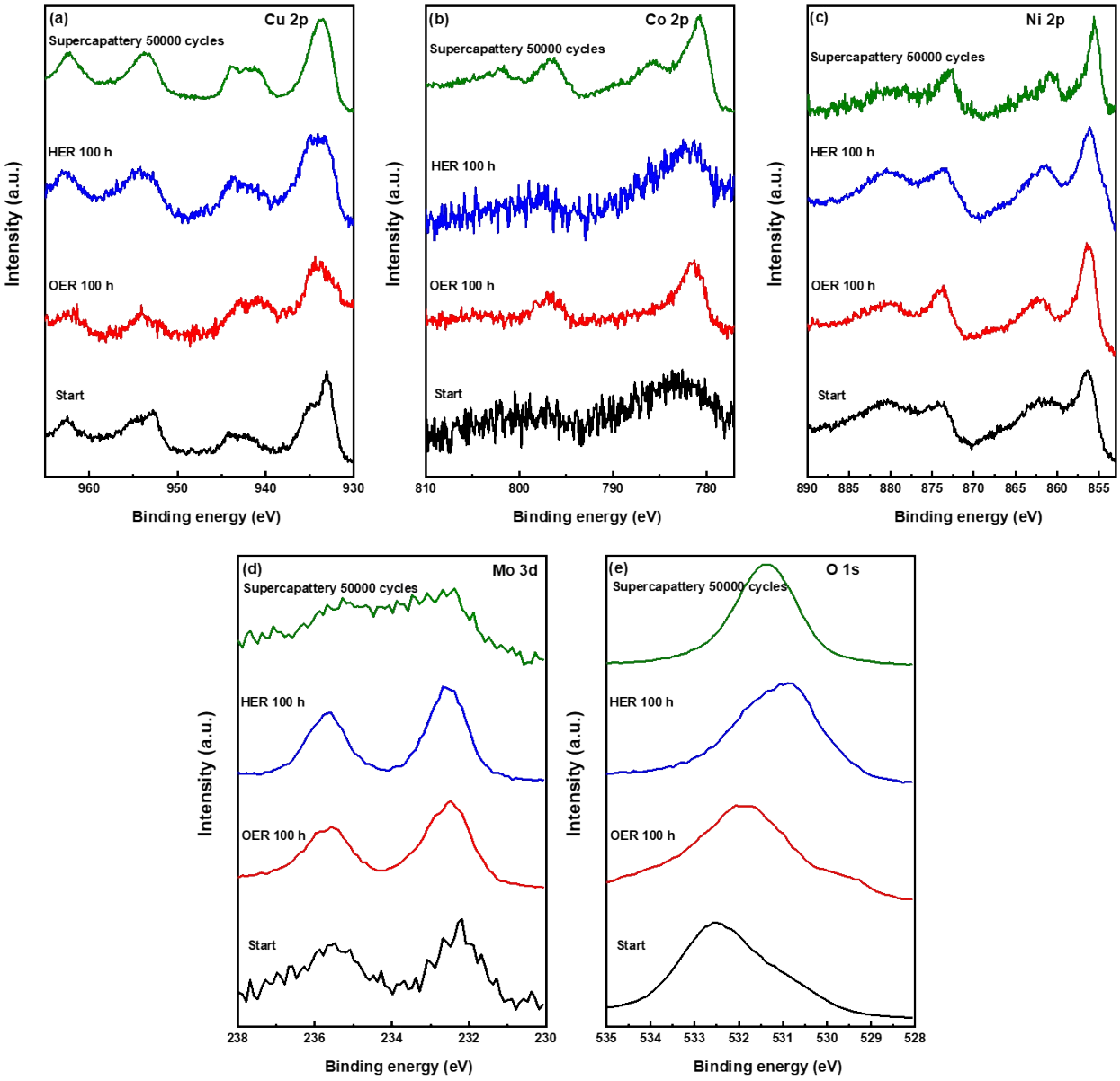
(a)
Cu 2p
Supercapattery 50000 cycles
HER 100 h
OER 100 h
Start
Intensity (a.u.)
960
950
940
930
Binding energy (eV)
(b)
Co 2p
Supercapattery 50000 cycles
HER 100 h
OER 100 h
Start
Intensity (a.u.)
810
800
790
780
Binding energy (eV)
(c)
Ni 2p
Supercapattery 50000 cycles
HER 100 h
OER 100 h
Start
Intensity (a.u.)
890
885
880
875
870
865
860
855
Binding energy (eV)
(d)
Mo 3d
Supercapattery 50000 cycles
HER 100 h
OER 100 h
Start
Intensity (a.u.)
238
236
234
232
230
Binding energy (eV)
(e)
O 1s
Supercapattery 50000 cycles
HER 100 h
OER 100 h
Start
Intensity (a.u.)
535
534
533
532
531
530
529
528
Binding energy (eV)

**Figure S6.** XPS spectra of a) Cu 2p, b) Co 2p, c) Ni 2p, d) Mo 3d and e) O 1s for NiO@$CuCo_2O_4$/MoNi heterostructure before and after OER, HER, and supercapattery test.

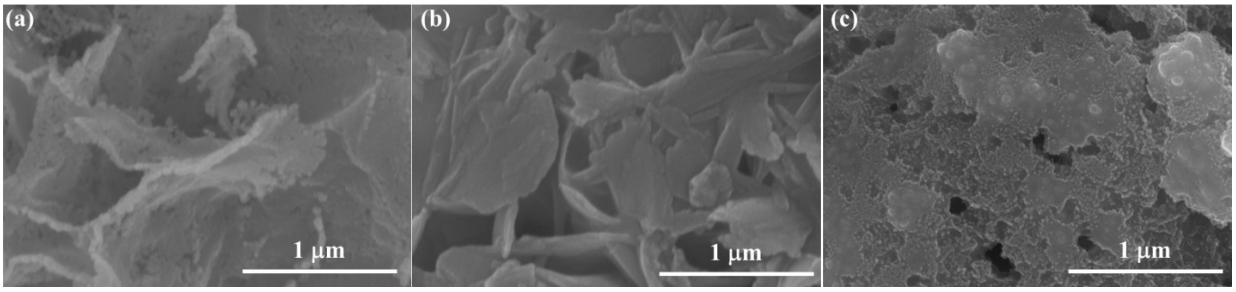


**Figure S7.** FE-SEM images of the NiO@$CuCo_2O_4$/MoNi heterostructure after a) OER, b) HER, and c) supercapattery test.

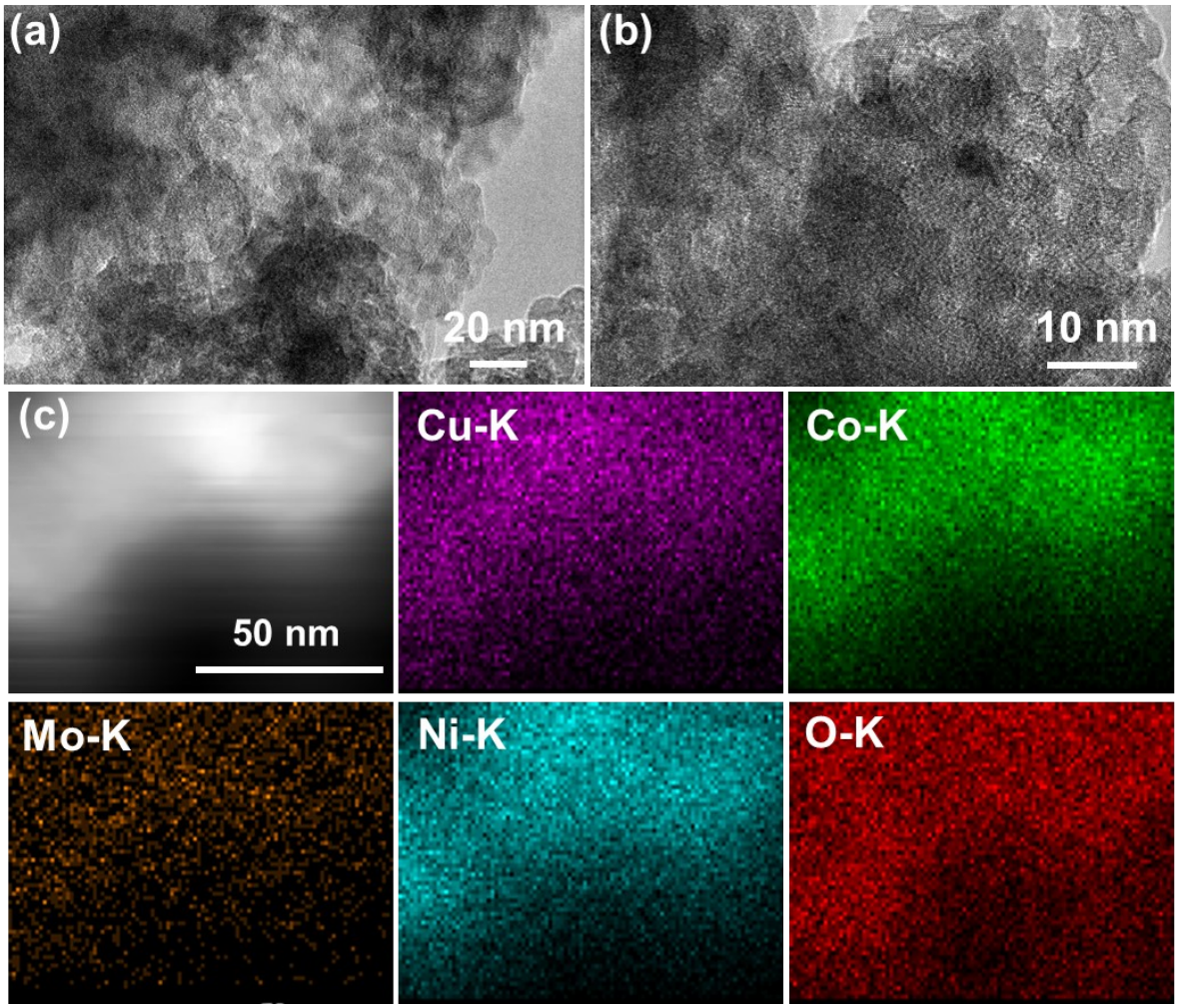
(a)
20 nm
(b)
10 nm
(c)
50 nm
Cu-K
Co-K
Mo-K
Ni-K
O-K

**Figure S8.** HR-TEM images of the NiO@$CuCo_2O_4$/MoNi heterostructure after a, b) HER test and c) the corresponding elemental mapping of NiO@$CuCo_2O_4$/MoNi heterostructure.

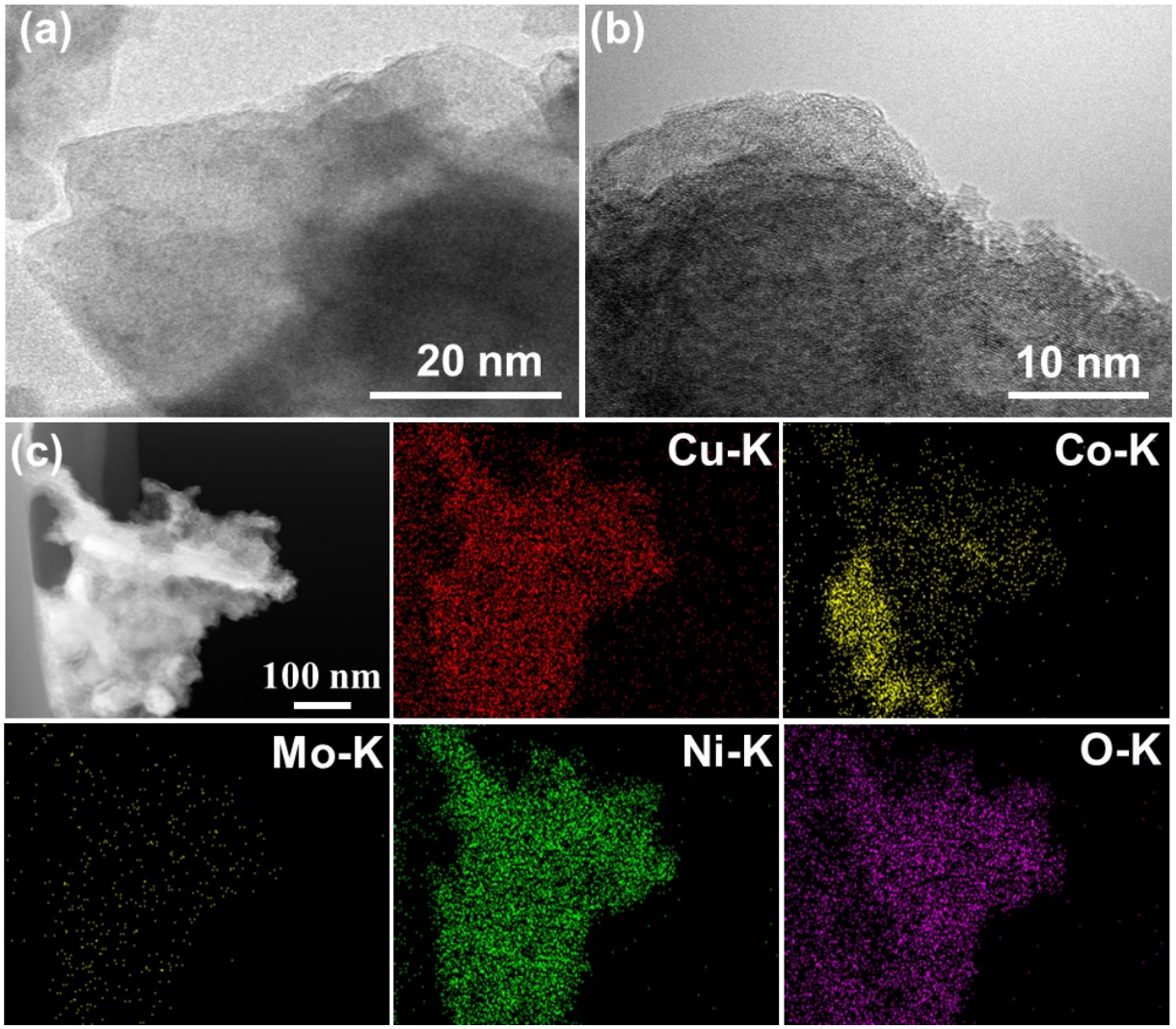


**Figure S9.** HR-TEM images of the NiO@$CuCo_2O_4$/MoNi heterostructure after a, b) OER test and c) the corresponding elemental mapping of NiO@$CuCo_2O_4$/MoNi heterostructure.

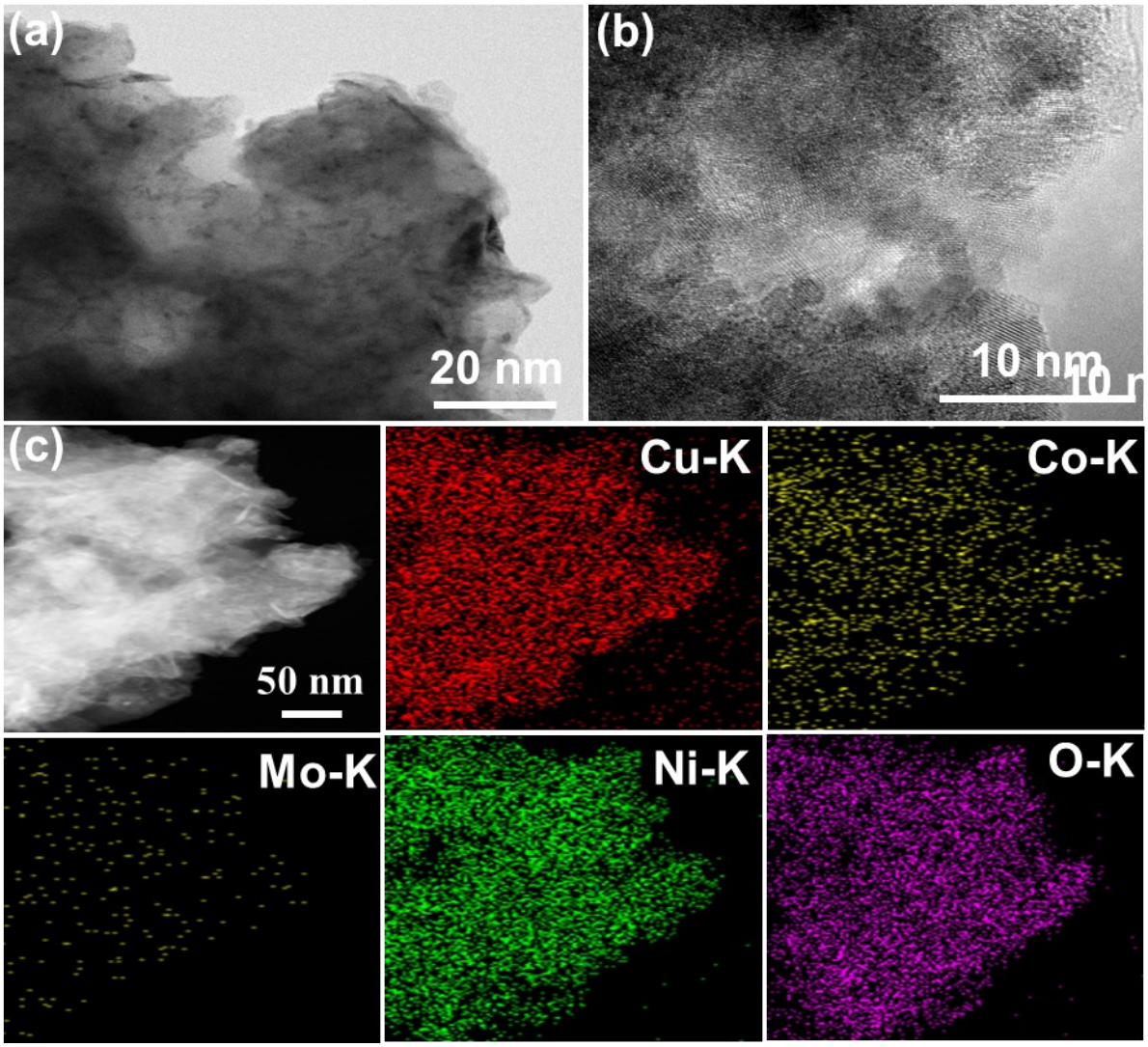
(a)
20 nm
(b)
10 nm
(c)
50 nm
Cu-K
Co-K
Mo-K
Ni-K
O-K

**Figure S10.** HR-TEM images of the NiO@$CuCo_2O_4$/MoNi heterostructure after a, b) 50000 cycling test and c) the corresponding elemental mapping of NiO@$CuCo_2O_4$/MoNi heterostructure.

**Table S1.** Comparison of HER performances of NiO@$CuCo_2O_4$/MoNi heterostructure with other reported electrocatalysts.

| **Catalyst** | **Electrolyte** | **Overpotential at 50 mA $cm^{-2}$ (mV)** | **Tafel slope (mV $dec^{-1}$)** | **Ref.** |
|---|---|---|---|---|
| NiO@$CuCo_2O_4$/MoNi heterostructure | 1 M KOH | 61.0 | 44.2 | This work |
| NiMoOx/NiMoS | 1 M KOH | ~63 | - | [4] |
| $MoS_2/Ni_3S_2$ | 1 M KOH | ~175 | - | [5] |
| $NiCo_2O_4$@$NiMoO_4$ | 1 M KOH | 300 | 94.0 | [6] |
| $NiCo_2O_4$@$Ni_{0.796}$CoLDH | 1 M KOH | 115 | 56.4 | [7] |
| FeOOH/$NiCo_2O_4$ | 1 M KOH | 146 | 41.3 | [8] |
| $Ni(OH)_2$@CuS | 1 M KOH | 95 | 42.0 | [9] |
| H-Fe-CoMoS | 1 M KOH | 138 | 98.0 | [10] |
| Co/$Co_2Mo_3O_8$ | 1 M KOH | ~110 | - | [11] |
| NiFe-LDH/$NiCo_2O_4$ | 1 M KOH | 192 | 59.0 | [12] |
| $Ni_3N$/Pt | 1 M KOH | 83 | - | [13] |
| Mo-NiCoP | 1 M KOH | 121 | - | [14] |
| $NiCo_2O_4$@$CoMoO_4$ | 1 M KOH | 121 | 77.0 | [15] |

**Table S2.** Comparison of OER performances of $NiO@CuCo_2O_4/MoNi$ heterostructure with other reported electrocatalysts.

| **Catalyst** | **Electrolyte** | **Overpotential at 100 mA cm$^{-2}$ (mV)** | **Tafel slope (mV dec$^{-1}$)** | **Ref.** |
|---|---|---|---|---|
| $NiO@CuCo_2O_4/MoNi$ heterostructure | 1 M KOH | 370 | 69.1 | This work |
| $NiCo_2O_4@CoMoO_4$ | 1 M KOH | ~490 | - | [15] |
| $NiCo_2O_4@NiMoO_4$ | 1 M KOH | ~420 | - | [16] |
| $Fe_2O_3@CuO$ NTs | 1 M KOH | ~380 | - | [17] |
| Ni@Co-Ni-P | 1 M KOH | 380 | 65 | [18] |
| $Co_3O_4/NiCo_2O_4$ | 1 M KOH | 495 | 88 | [19] |
| NiCoFe phosphate NSs-C | 1 M KOH | ~350 | - | [20] |
| $Ni_2P$@NF-6 | 1 M KOH | 590 | 297 | [21] |
| p-$Cu_{1-x}NNi_{3-y}$/FeNiCu | 1 M KOH | ~350 | - | [22] |
| NiCoP NWAs/NF | 1 M KOH | ~320 | - | [23] |

**Table S3.** Comparison of water splitting performance of $NiO@CuCo_2O_4/MoNi$ heterostructure with other reported bi-functional electrocatalysts based on transition metals.

| Catalyst | Electrolyte | Voltage (V) | Ref. |
|---|---|---|---|
| $NiO@CuCo_2O_4/MoNi$ heterostructure | 1 M KOH | 1.54 V @ 10 mA $cm^{-2}$ | This work |
| E-Mo-NiCoP | 1 M KOH | 1.61 V @ 10 mA $cm^{-2}$ | 14 |
| $FeCo_2S_4$ | 1 M KOH | 1.56 V @ 10 mA $cm^{-2}$ | 24 |
| $NiSe/Ni_3Se_2$ | 1 M KOH | 1.6 V @ 10 mA $cm^{-2}$ | 25 |
| $NiS-Ni_2P_2S_6$ | 1 M KOH | 1.64 V @ 10 mA $cm^{-2}$ | 26 |
| $NiFe/NiCo_2O_4$ | 1 M KOH | 1.67 V @ 10 mA $cm^{-2}$ | 27 |
| $NiCo_2O_4/NiCoP$ | 1 M KOH | 1.66 V @ 10 mA $cm^{-2}$ | 28 |
| $Ni_3S_2$ | 1 M KOH | 1.57 V @ 10 mA $cm^{-2}$ | 29 |
| Ni/NiO | 1 M KOH | 1.71 V @ 10 mA $cm^{-2}$ | 30 |
| $CoxPO_4/CoP$ | 1 M KOH | 1.91 V @ 10 mA $cm^{-2}$ | 31 |
| $Co_9S_8-CoSe_2$ | 1 M KOH | 1.66 V @ 10 mA $cm^{-2}$ | 32 |
| $MoP@Ni_3P/NF$ | 1 M KOH | 1.67 V @ 10 mA $cm^{-2}$ | 33 |

**Table S4.** Summary of electrochemical performance of transition metal oxide heteronanostructure reported in literature.

| **Material** | **Fabrication method** | **Current Collector** | **Electrolyte** | **$C_s$ F $g^{-1}$ (Current density A $g^{-1}$)** | **Stability (Cycles)** | **Ref.** |
|---|---|---|---|---|---|---|
| NiO@$CuCo_2O_4$/MoNi heterostructure | Hydrothermal/ ALD | NF | 2 M KOH | 3527.7 F $g^{-1}$ (1587.5 C $g^{-1}$) (1 A $g^{-1}$) | 84.2% (50000) | This work |
| $Cu_2O$@$Mn(OH)_2$ | Solvent process | NF | 2 M KOH | 647.2 F $g^{-1}$ (0.5 A $g^{-1}$) | 71.5% (3000) | [34] |
| $CuCo_2O_4$/$MnCo_2O_4$ | Hydrothermal | NF | 2 M KOH | 1434 F $g^{-1}$ (0.5 A $g^{-1}$) | 98.4% (5000) | [35] |
| $CuCo_2O_4$@$Ni(OH)_2$ | Hydrothermal and Electrodeposition | NF | 6 M KOH | 1902.0 F $g^{-1}$ (2 A $g^{-1}$) | 87.6% (50000) | [36] |
| $CuCo_2O_4$/$NiMoO_4$ | Hydrothermal | NF | 3 M KOH | 2215.0 F $g^{-1}$ (1 A $g^{-1}$) | 98% (8000) | [37] |

| | | | | | | |
|---|---|---|---|---|---|---|
| $CoMoS@Co(OH)_2$ | Hydrothermal and calcination | Carbon cloth | 3M KOH | 1711.0 F $g^{-1}$ (20 mA $cm^{-2}$) | 90.3% (5000) | 38 |
| $CuCo_2O_4@Co(OH)_2$ | Hydrothermal | NF | 1 M KOH | 375.0 F $g^{-1}$ (1 A $g^{-1}$) | 85.8% (10000) | 39 |
| $CuCo_2O_4$/CuO nanowire | Hydrothermal | NF | 2 M KOH | 642.0 F $g^{-1}$ (1 A $g^{-1}$) | 88% (5000) | 40 |
| NiO/$NiCo_2O_4$/$Co_3O_4$ | sol-gel process and calcination | NF | 2M KOH | 1600.0 F $g^{-1}$ (2.5 A $g^{-1}$) | 94.9% (1000) | 41 |
| $Co_3O_4$@CoNi-LDH | Hydrothermal | NF | 2M KOH | 2676.9 F $g^{-1}$ (0.5 A $g^{-1}$) | 67.7% (10000) | 42 |
| $CuCo_2O_4@Ni(OH)_2$ | Hydrothermal and Chemical deposition | Carbon fiber cloth | 2 M KOH | 2160.0 F $g^{-1}$ (5 A $g^{-1}$) | 92% (5000) | 43 |
| $CuCo_2O_4$ NWs@$NiMoO_4$ | Hydrothermal | NF | 6 M KOH | 2207.0 F $g^{-1}$ (1.25 A $g^{-1}$) | 95.6% (5000) | 44 |
| $CuCo_2O_4$/NiO nanotrees | Hydrothermal and | NF | 1 M NaOH | 2219.0 F $g^{-1}$ | 95.3% | 45 |

| | | | | | | |
|---|---|---|---|---|---|---|
| | Chemical bath deposition | | | (1 A $g^{-1}$) | (10000) | |

**Table S5.** Comparison of energy storage performance of various Cu and Co-based HSCs.

| **HSC devices** | **Cell voltage (V)** | **Electrolyte** | **$C_s$/F $g^{-1}$ (Current density A $g^{-1}$)** | **Stability (Cycles)** | **Energy density (W h $kg^{-1}$)** | **Power density (W $kg^{-1}$)** | **Ref.** |
|---|---|---|---|---|---|---|---|
| NiO@$CuCo_2O_4$/MoNi heterostructure//AC | 1.6 | KOH | 226.7 F $g^{-1}$ (362.8 C $g^{-1}$) (1 A $g^{-1}$) | 90.4% (25000) | 80.6 | 692.8 | This work |
| $CuCo_2O_4$/CuO//RGO/$Fe_2O_3$ | 1.6 | KOH | 93.0 F $g^{-1}$ (0.25 A $g^{-1}$) | 83.0% (5000) | 33.0 | 200.0 | [40] |
| $Co_3O_4$@CoNi-LDH//AC | 1.5 | KOH | 195.9 F $g^{-1}$ (1 A $g^{-1}$) | 103.5% (5000) | 61.2 | 750 | [42] |
| $CuCo_2O_4$/$MnCo_2O_4$//graphene | 1.6 | KOH | 118.4 F $g^{-1}$ (0.5 A $g^{-1}$) | 88.4% (10000) | 42.1 | 400.0 | [35] |
| $CuCo_2O_4$/$NiMoO_4$//AC | 1.5 | KOH | ~140.0 F $g^{-1}$ (1 A $g^{-1}$) | 89% (5000) | 44.8 | 374.2 | [37] |
| $CuCo_2O_4$@$NiMoO_4$//AC | 1.6 | KOH | 128.2 F $g^{-1}$ | 80.2 % | 40.0 | - | [44] |

| | | | | | | | |
|---|---|---|---|---|---|---|---|
| | | | (1 A $g^{-1}$) | (5000) | | | |
| CNTs@NCDHNs//rGO-$Fe_2O_3$ | 1.6 | KOH | 108.7 F $g^{-1}$ (1 A $g^{-1}$) | ~93.5% (1000) | 54.6 | 1130.0 | [46] |
| NiCo-LDH/NiMoSx// $Fe_2O_3$/rGO | 1.6 | KOH | 203.9 F $g^{-1}$ (3 mA $cm^{-2}$) | 91.5% (10000) | 72.6 | 522.7 | [47] |
| $CuCo_2O_4$/NiO//AC | 1.6 | NaOH | 155.0 F $g^{-1}$ (1 A $g^{-1}$) | 91.5% (5000) | 51.8 | 866.0 | [45] |
| $CuCo_2O_4$@$MnMoO_4$//graphene | 1.6 | KOH | 165.7 F $g^{-1}$ (1 A $g^{-1}$) | 92 .5% (6000) | 58.9 | 670.0 | [48] |
| $CuCo_2O_4$@PPy//Carbon | 1.4 | KOH | 208.0 F $g^{-1}$ (2 A $g^{-1}$) | 92 % (5000) | 52.0 | 748.0 | [49] |
| $CuCo_2O_4$@$Ni(OH)_2$//AC | 1.6 | KOH | 108.5 F $g^{-1}$ (1 A $g^{-1}$) | 93.7% (5000) | 38.6 | 800.0 | [36] |
| CuCo2S4/CuCo2O4//graphene | 1.6 | KOH | 90.4 F $g^{-1}$ (1 A $g^{-1}$) | 73.0% (5000) | 33.2 | 800.0 | [50] |

## References


1. T. Kavinkumar, S. Seenivasan, H. H. Lee, H. Jung, J. W. Han and D.-H. Kim, *Nano Energy*, 2021, **81**, 105667.
2. Y. Z. Chen, T. F. Zhou, L. Li, W. K. Pang, X. M. He, Y. N. Liu and Z. P. Guo, *ACS Nano*, 2019, **13**, 9376-9385.
3. S. L. Zhang and N. Pan, *Adv. Energy Mater.*, 2015, **5,** 1401401.
4. P. L. Zhai, Y. X. Zhang, Y. Z. Wu, J. F. Gao, B. Zhang, S. Y. Cao, Y. T. Zhang, Z. W. Li, L. C. Sun and J. G. Hou, *Nat. Commun.*, 2020, **11,** 5462.
5. J. Zhang, T. Wang, D. Pohl, B. Rellinghaus, R. H. Dong, S. H. Liu, X. D. Zhuang and X. L. Feng, *Angew. Chem. Int. Ed.*, 2016, **55**, 6702-6707.
6. D. Cui, R. D. Zhao, J. Q. Dai, J. Xiang and F. F. Wu, *Dalton T.*, 2020, **49**, 9668-9679.
7. M. Li, L. Tao, X. Xiao, X. Jiang, M. Wang and Y. Shen, *ACS Sustain. Chem. Eng.*, 2019, **7**, 4784-4791.
8. X. Cao, Y. Sang, L. Wang, G. Ding, R. Yu and B. Geng, *Nanoscale*, 2020, **12**, 19404-19412.
9. S. Q. Liu, H. R. Wen, Ying-Guo, Y. W. Zhu, X. Z. Fu, R. Sun and C. P. Wong, *Nano Energy*, 2018, **44**, 7-14.
10. Y. N. Guo, X. Zhou, J. Tang, S. Tanaka, Y. V. Kaneti, J. Na, B. Jiang, Y. Yamauchi, Y. S. Bando and Y. Sugahara, *Nano Energy*, 2020, **75**.
11. M. J. Zang, N. Xu, G. X. Cao, Z. J. Chen, J. Cui, L. Y. Gan, H. B. Dai, X. F. Yang and P. Wang, *ACS Catal.*, 2018, **8**, 5062.
12. Z. Q. Wang, S. Zeng, W. H. Liu, X. W. Wang, Q. W. Li, Z. G. Zhao and F. X. Geng, *ACS Appl. Mater. Interfaces*, 2017, **9**, 1488-1495.

13. Y. H. Wang, L. Chen, X. M. Yu, Y. G. Wang and G. F. Zheng, *Adv. Energy Mater.*, 2017, **7,** 1601390.

14. J. H. Lin, Y. T. Yan, C. Li, X. Q. Si, H. H. Wang, J. L. Qi, J. Cao, Z. X. Zhong, W. D. Fei and J. C. Feng, *Nano-Micro Lett.*, 2019, **11,** 3676.

15. Y. Q. Gong, Z. Yang, Y. Lin, J. L. Wang, H. L. Pan and Z. F. Xu, *J. Mater. Chem. A*, 2018, **6**, 16950-16958.

16. X. Q. Du, J. P. Fu and X. S. Zhang, *Chemcatchem.*, 2018, **10**, 5533-5540.

17. Y. Gao, N. Zhang, C. R. Wang, F. Zhao and Y. Yu, *ACS Appl. Energ. Mater.*, 2020, **3**, 666-674.

18. W. Li, X. F. Gao, X. G. Wang, D. H. Xiong, P. P. Huang, W. G. Song, X. Q. Bao and L. F. Liu, *J. Power Sources*, 2016, **330**, 156-166.

19. H. Hu, B. Y. Guan, B. Y. Xia and X. W. Lou, *J. Am. Chem. Soc.*, 2015, **137**, 5590-5595.

20. M. A. Z. G. Sial, H. F. Lin and X. Wang, *Nanoscale*, 2018, **10**, 12975-12980.

21. J. L. Zheng, W. Zhou, T. Liu, S. J. Liu, C. B. Wang and L. Guo, *Nanoscale*, 2017, **9**, 4409-4418.

22. Y. P. Zhu, G. Chen, Y. J. Zhong, Y. B. Chen, N. N. Ma, W. Zhou and Z. P. Shao, *Nat. Commun.*, 2018, **9,** 2326.

23. J. Z. Li, G. D. Wei, Y. K. Zhu, Y. L. Xi, X. X. Pan, Y. Ji, I. V. Zatovsky and W. Han, *J. Mater. Chem. A*, 2017, **5**, 14828-14837.

24. J. R. Hu, Y. Q. Ou, Y. H. Li, D. Gao, Y. H. Zhang and P. Xiao, *ACS Sustain. Chem. Eng.*, 2018, **6**, 11724-11733.

25. F. F. Zhang, Y. Pei, Y. C. Ge, H. Chu, S. Craig, P. Dong, J. Cao, P. M. Ajayan, M. X. Ye and J. F. Shen, *Adv. Mater. Interfaces*, 2018, **5,** 1701507.

26. X. Y. Zhang, S. Zhang, J. Li and E. K. Wang, *J. Mater. Chem. A*, 2017, **5**, 22131-22136.

27. C. L. Xiao, Y. B. Li, X. Y. Lu and C. Zhao, *Adv. Funct. Mater.*, 2016, **26**, 3515-3523.

28. W. Jin, J. P. Chen, H. B. Wu, N. Zang, Q. W. Li, W. Q. Cai and Z. X. Wu, *Catal. Sci.Technol.*, 2020, **10**, 5559-5565.

29. J. F. Zhang, Y. Li, T. Y. Zhu, Y. Wang, J. W. Cui, J. J. Wu, H. Xu, X. Shu, Y. Q. Qin, H. M. Zheng, P. M. Ajayan, Y. Zhang and Y. C. Wu, *ACS Appl. Mater. Interfaces* 2018, **10**, 31330-31339.

30. H. Sun, Z. Ma, Y. Qiu, H. Liu and G.-g. Gao, *Small*, 2018, **14**, 1800294.

31. Y. Yang, H. L. Fei, G. D. Ruan and J. M. Tour, *Adv. Mater.*, 2015, **27**, 3175-3180.

32. S. Chakrabartty, S. Karmakar and C. R. Raj, *ACS Appl. Nano Mater.*, 2020, **3**, 11326-11334.

33. F. M. Wang, J. W. Chen, X. P. Qi, H. Yang, H. H. Jiang, Y. Q. Deng and T. X. Liang, *Appl. Surf. Sci.* 2019, **481**, 1403-1411.

34. H. Guan, P. Cai, X. Zhang, Y. Zhang, G. Chen and C. Dong, *J. Mater. Chem. A*, 2018, **6**, 13668-13675.

35. S. Liu, K. S. Hui, K. N. Hui, J. M. Yun and K. H. Kim, *J. Mater. Chem. A*, 2016, **4**, 8061-8071.

36. W. Liu, H. Chen, H. Liao, K. Xiang, W. Chen and X. Li, *Ind. Eng. Chem. Res.*, 2019, **58**, 21233-21241.

37. G. F. Li, B. Song, X. Cui, H. Z. Ouyang, K. L. Wang, Y. M. Sun and Y. Q. Wang, *ACS Sustain. Chem. Eng.*, 2020, **8**, 1687-1694.

38. S. J. Patil and D.-W. Lee, *J. Mater. Chem. A*, 2018, **6**, 9592-9603.

39. Y. Zhang, H. Liu, M. Huang, J. M. Zhang, W. Zhang, F. Dong and Y. X. Zhang, *Chemelectrochem.*, 2017, **4**, 721-727.

40. Y. Wang, C. Shen, L. Niu, R. Li, H. Guo, Y. Shi, C. Li, X. Liu and Y. Gong, *J. Mater. Chem. A*, 2016, **4**, 9977-9985.

41. M. C. Liu, L. B. Kong, C. Lu, X. M. Li, Y. C. Luo and L. Kang, *ACS Appl. Mater. Interfaces*, 2012, **4**, 4631-4636.

42. J.-J. Zhou, Q. Li, C. Chen, Y.-L. Li, K. Tao and L. Han, *Chem. Eng. J.*, 2018, **350**, 551-558.

43. D. Zhu, X. Sun, J. Yu, Q. Liu, J. Y. Liu, R. R. Chen, H. S. Zhang, R. M. Li, J. Yu and J. Wang, *J. Colloid Interf. Sci.*, 2019, **557**, 76-83.

44. J. H. Lin, H. Y. Liang, H. N. Jia, S. L. Chen, Y. F. Cai, J. L. Qi, J. Cao, W. D. Fei and J. C. Feng, *Inorg. Chem. Front.*, 2017, **4**, 1575-1581.

45. K. W. Qiu, M. Lu, Y. S. Luo and X. W. Du, *J. Mater. Chem. A*, 2017, **5**, 5820-5828.

46. Y. Wang, H. L. Wei, H. F. Lv, Z. X. Chen, J. J. Zhang, X. Y. Yan, L. Lee, Z. M. M. Wang and Y. L. Chueh, *ACS Nano*, 2019, **13**, 11235-11248.

47. S. Kandula, K. R. Shrestha, G. Rajeshkhanna, N. H. Kim and J. H. Lee, *ACS Appl. Mater. Interfaces*, 2019, **11**, 11555-11567.

48. S. Chen, S. Cui, S. Chandrasekaran, C. Ke, Z. Li, P. Chen, C. Zhang and Y. Jiang, *Electrochim. Acta*, 2020, **341**, 135893.

49. R. BoopathiRaja, M. Parthibavarman and A. N. Begum, *Mater. Res. Bull.*, 2020, **126,** 110817.

50. X. Xu, Y. Liu, P. Dong, P. M. Ajayan, J. Shen and M. Ye, *J. Power Sources*, 2018, **400**, 96-103.